

Ideal Taper Prediction for Slab Casting

Brian G. Thomas and Claudio Ojeda
Mechanical and Industrial Engineering Department
University of Illinois at Urbana-Champaign
1206 W. Green St., Urbana, IL 61801, USA
Tel.:217-244-2859, E-mail: bgthomas@uiuc.edu

Key Words: Continuous casting, Computational model, Heat flux, Thermal shrinkage, Solidification, Ideal taper, Mold distortion, Casting speed, Powder properties, Steel grade, Automated width change

INTRODUCTION

The design and operation of a continuous casting mold to consistently produce high quality steel requires careful selection and control of many variables, such as mold oscillation^[1], powder practice, heat transfer and taper, according to the casting speed, steel grade, section size, and other conditions^[2,3]. Manfred Wolf was the most knowledgeable student of this complex subject of continuous casting of steel that the world has ever known. He devoted his career to identifying technologies to achieve these objectives and communicating them to those who could make a difference. Taper is one of these important practices, and is the subject of this paper.

During continuous casting of steel slabs, the mold walls must be tapered such that they remain in contact with the solidifying steel shell while it cools and shrinks. This is done by relative movement of the upper and lower screw adjustments to change the angle of hotface slope of the narrowface. Taper is measured before and after casting with hand-held gages and should be monitored during operation using inclinometers. Proper taper ensures uniform heat transfer between the mold and steel surfaces, without exerting excessive contact forces on the hot and weak shell. Insufficient taper causes reduced heat flux across the mold/strand interface, leading to a thinner, weaker shell^[4]. This may cause breakouts, where liquid steel bursts through the shell, or bulging below mold, which leads to longitudinal quality problems such as off-corner “gutter” and subsurface longitudinal cracks^[5]. Excessive taper also causes many problems, including mold wear, friction leading to axial tensile stress causing transverse cracks, and even buckling of the wide face shell, gutter and associated problems^[6].

Several efforts have been conducted to predict ideal mold taper in previous work^[6-11]. These include simulations of square billets,^[7, 11] round billets,^[10] and slabs^[6, 9]. None has quantitatively investigated the effect of casting conditions on ideal taper. In this work, shell shrinkage is predicted using a finite element elastic-viscoplastic thermal-stress model of the continuous casting process. Ideal tapers are then predicted for different casting speeds, working mold lengths, steel grades and mold fluxes.

Basic mold taper calculation – Taper of the narrowface mold walls is needed to compensate for shrinkage of the wide face shell, which is caused mainly by thermal strain controlled by mold heat transfer. Wideface taper, due to shrinkage of the narrow face, is not as critical because the long, unsupported shell will always bulge under ferrostatic pressure to contact the wide face, except for very near the corners. Narrowface taper is defined

by the horizontal shift in position of each mold plate, ΔW , per strand width, W , (Eq. 1), or by dividing this result by mold length, L , (Eq. 2). Care should be taken not to confuse which of the two methods is used, (percent per mold, or percent per unit length).

$$taper(\%) = 2 \frac{\Delta W}{W} \cdot 100\% \quad (1)$$

$$taper(\%/m) = 2 \frac{\Delta W}{LW} \cdot 100\% \quad (2)$$

Ideal taper is affected by mold heat transfer, casting speed, steel grade, powder composition and other variables. Taper due to thermal shrinkage of the wideface can be crudely estimated by multiplying the drop in shell surface temperature between the top and bottom of the mold (1500-1000°C in Fig. 1) by the thermal expansion coefficient (about 0.002%/°C). This equals 1%/mold, which is typical narrowface taper. Further improvement requires consideration of the heat removal distribution down the mold, mold distortion, interfacial flux layer behavior, mold contour in a funnel-shaped mold, and dynamic effects during automatic width change.

THERMAL SHRINKAGE MODEL

A finite-element elastic-viscoplastic thermal-stress model, CON2D [12-14] was applied to investigate ideal taper of slab molds by predicting shrinkage of the solidifying steel shell. The model solves a 2D finite-element discretization of the transient heat conduction equation in a Lagrangian reference frame that moves down through the caster with the solidifying steel shell. Next, the force equilibrium, constitutive, and strain displacement equations are solved under a condition of generalized plane strain in both the width and casting directions [12]. Thermal and mechanical behavior are studied here in a longitudinal slice through the centerline of the shell (Fig. 2). This slice domain has been shown to be an accurate and economical method to approximate taper, despite the corner effects [11].

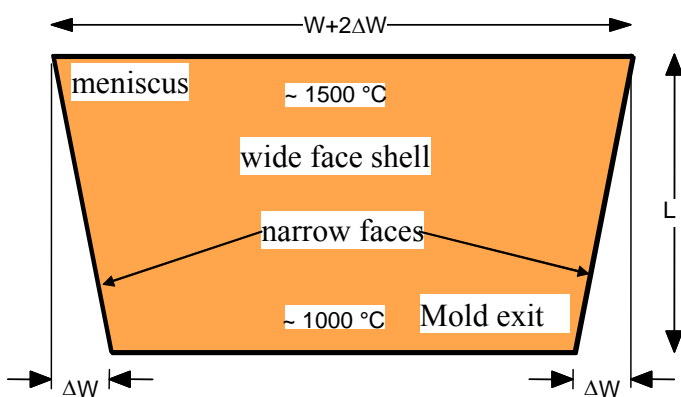


Fig. 1: Wide face shrinkage and narrowface taper

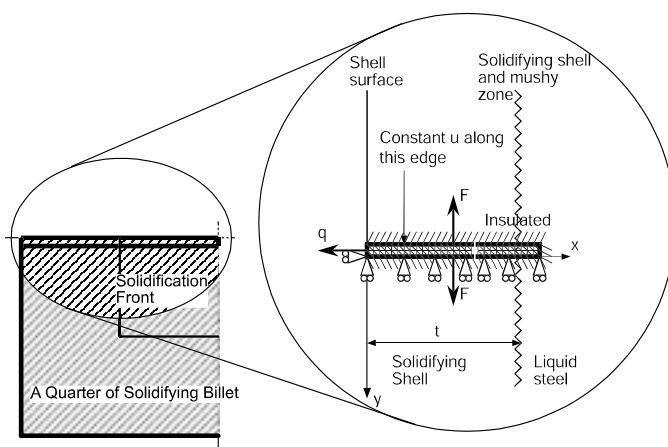


Fig. 2: 1-D Slice Simulation Domain for CON2D

Heat Flow Model – Heat flux leaving the surface of the solidifying shell is calculated using a finite-difference model of shell solidification, CON1D, that features detailed treatment of the slag layers in the interfacial gap, coupled to a 2-D computation of mold heat conduction [15]. Typical CON1D predictions are compared in Fig. 3 with measurements from a variety of sources, including those compiled by Manfred Wolf [2]. For high carbon steel simulations, the instantaneous heat flux is obtained as a function of mold residence time by differentiating the curve fit of average mold heat extraction measurements given elsewhere [14].

The total heat flux (integrated from the heat flux profile) was forced to match Eq. 3 [16], which was obtained from a curve fit of many measurements under different conditions at a typical slab caster [16].

$$Q_G = 4.63 \cdot 10^6 \mu^{-0.09} T_{flow}^{-1.19} V_C^{0.47} \left\{ 1 - 0.152 \exp \left[- \left(\frac{0.107 - \%C}{0.027} \right)^2 \right] \right\} \quad (3)$$

Where Q_G is the mean heat flux (MW/m^2), μ is the powder viscosity at $1300\text{ }^\circ\text{C}$, (Pa-s), T_{flow} is the melting temperature of the mold flux ($^\circ\text{C}$), V_C is the casting speed (m/min), and $\%C$ is the carbon content. This equation quantifies the well-known facts (documented by Wolf^[3]) that heat flux drops for peritectic steels (near $.107\%C$) and for mold powders with high solidification temperatures, (which hence form a thicker insulating flux layer against the mold wall). There is also a very slight drop in heat flux for mold powders with higher viscosity. This equation produces results similar to other measurements, as shown in Fig. 3 (800mm working mold length for Table I conditions for $0.07\%C$ steel)

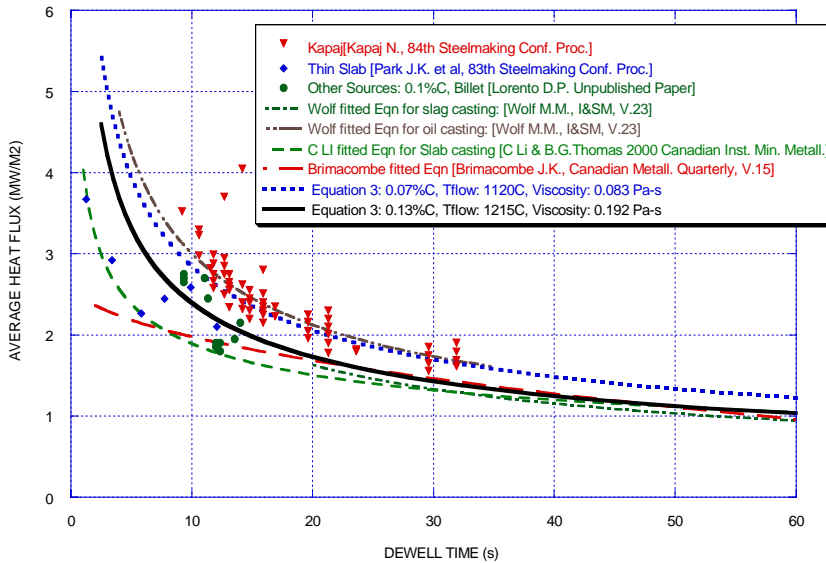


Fig. 3: Measured Average Mold Heat Flux

Kozlowski^[17] was applied. This function matches tensile test measurements of Wray^[18] and creep test data of Suzuki^[19]. When the steel contains significant amounts of soft delta-ferrite phase ($\% \delta > 10\%$), a power-law model is used^[14], which matches measurements of Wray above $1400\text{ }^\circ\text{C}$ ^[20]. Fig. 5 shows the accuracy of the constitutive model predictions compared with stresses measured by Wray^[18] at 5% strain at different strain rates and temperatures. This figure also shows the higher relative strength of austenite, which is important for

Stress Model - The total strain is composed of elastic, thermal, inelastic and flow-strain components. Thermal strain dominates the total, and depends on temperature and steel grade, as shown in Fig. 4. Unified plastic-creep constitutive models are used to capture the temperature, strain-rate, phase fraction, and grade sensitivity of steel strength at high temperature. The instantaneous equivalent inelastic strain rate depends on the current equivalent stress, temperature, the carbon content, and the current equivalent inelastic strain, which accumulates below the solidus temperature. When the steel is mainly austenite phase, ($\% \gamma > 90\%$), Model III by

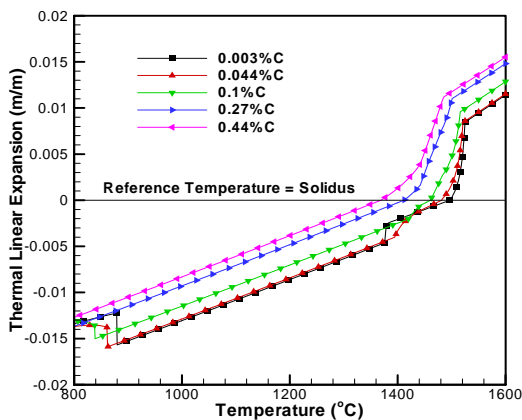


Fig. 4: Thermal expansion of steel

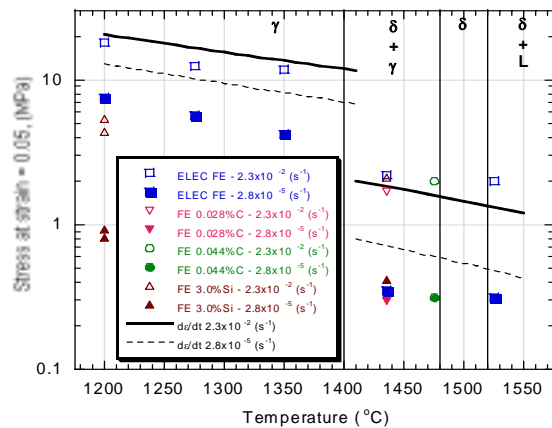


Fig. 5: Steel strength at high temperature (comparing predicted and measured values for α and γ)

shrinkage of the solidifying shell, and greatly affects the grade dependence of ideal taper. Further details regarding the model formulation are presented elsewhere, including its extensive validation with both analytical solutions and plant measurements ^[11,14].

IDEAL TAPER CALCULATION

Several different phenomena influence ideal taper, which is calculated in this work with Eq. 1 by combining each contribution to the change in strand width, ΔW , relative to the mold wall position at ambient temperature:

$$\Delta W \text{ (mm)} = \Delta W_{\text{shell}} - \Delta W_{\text{NF-D}} - \Delta W_{\text{WF-E}} - \Delta W_{\text{WF-D}} - \Delta W_{\text{FUNNEL}} - \Delta W_{\text{FLUX}} \quad (4)$$

ΔW_{shell} is the decrease in width of the wideface due to shrinkage of the shell (mm), calculated with CON2D.

$\Delta W_{\text{NF-D}}$ is the narrow face distortion down the mold minus the distortion in the meniscus,

$\Delta W_{\text{WF-E}}$ is the wide face expansion at the meniscus minus the wide face expansion down the mold,

$\Delta W_{\text{WF-D}}$ is the wide face distortion,

ΔW_{FUNNEL} is decrease in wideface perimeter due to the change in mold cavity dimensions down a funnel mold,

ΔW_{FLUX} is the flux layer thickness down the mold minus that at the meniscus.

The distorted shape of a typical standard slab mold was computed with a 3-D finite element model ^[21] and is shown in Fig. 6, magnified fifty times. This distortion is estimated here using three components, for expansion of the wideface mold plates, distortion (bending) of the wideface, and narrowface distortion.

Narrow face distortion- The narrowface mold walls bend towards the molten steel, imparting curvature to the mold shape that helps to match the natural curved shrinkage profile of the solidifying shell. Narrowface distortion is estimated from the temperature differences between the hot and cold faces computed for the narrow face, such as shown in Fig. 8:

$$\Delta W_{\text{NF-D}} = \frac{3\alpha_{\text{hot}} \left(\bar{T}_{\text{hot}} - \bar{T}_{\text{cold}} \right) (t_{\text{hot}} + t_{\text{cold}})}{t_{\text{cold}}^2 K_1} [Lx - x^2] \quad (5)$$

$$\text{where: } K_1 = 4 + 6 \frac{t_{\text{hot}}}{t_{\text{cold}}} + 4 \left(\frac{t_{\text{hot}}}{t_{\text{cold}}} \right)^2 + \frac{E_{\text{hot}}}{E_{\text{cold}}} \left(\frac{t_{\text{hot}}}{t_{\text{cold}}} \right)^3 + \frac{E_{\text{cold}}}{E_{\text{hot}}} \frac{t_{\text{cold}}}{t_{\text{hot}}} \quad (6)$$

$\Delta W_{\text{NF-D}}$ is the narrowface distortion at a distance x below the top of the mold; t_{hot} and t_{cold} are the thicknesses of the hot and cold layers of the narrow face plate. An equivalent thickness is added to t_{cold} to account for the stiffness of the water jacket. E_{hot} and E_{cold} are the elastic modulus of the hot and cold layers; α_{hot} is the thermal expansion coefficient of the hot copper layer; L is the mold length. \bar{T}_{hot} and \bar{T}_{cold} are the averages of the linearized temperature profiles along the hot and cold faces, calculated with CON1D, as shown in Fig. 8. for a 700mm long mold (600 mm working length), t_{hot} of 35 mm and t_{cold} of 95 mm. These conditions and results reasonably match the 3-D model case in Fig. 6, where the maximum distortion is 1mm. For the standard slab caster studied here the mold length is 900mm (800 mm working length), t_{hot} is 35 mm and t_{cold} is 95 mm. For the thin slab caster, the mold length is 1100mm (1016mm working length), t_{hot} is 25 mm and t_{cold} is 221 mm.

Wide face expansion- If the narrow faces are clamped rigidly between the wide face mold plates, and backlash of the screws allows slight movement of the narrow faces, then differences in thermal expansion of the top and bottom of the widefaces during operation can cause affect mold taper. This wideface expansion is estimated from the mold temperatures obtained with CON1D using Eq. (7):

$$\Delta W_{\text{WF-E}} \text{ (mm)} = \alpha_{\text{mold}} \left(\frac{W}{2} \right) \left(T_{\text{ref}} - \frac{T_{\text{cold}} + T_{\text{hot}}}{2} \right) \quad (7)$$

Where α_{mold} is the thermal expansion coefficient of the copper, W is the wideface width, T_{cold} and T_{hot} are the linearized hot face and cold face temperatures, shown in Fig. 9. T_{ref} is the average linearized mold temperature at the meniscus, chosen to make $\Delta W_{\text{WF-E}}$ zero at the meniscus.

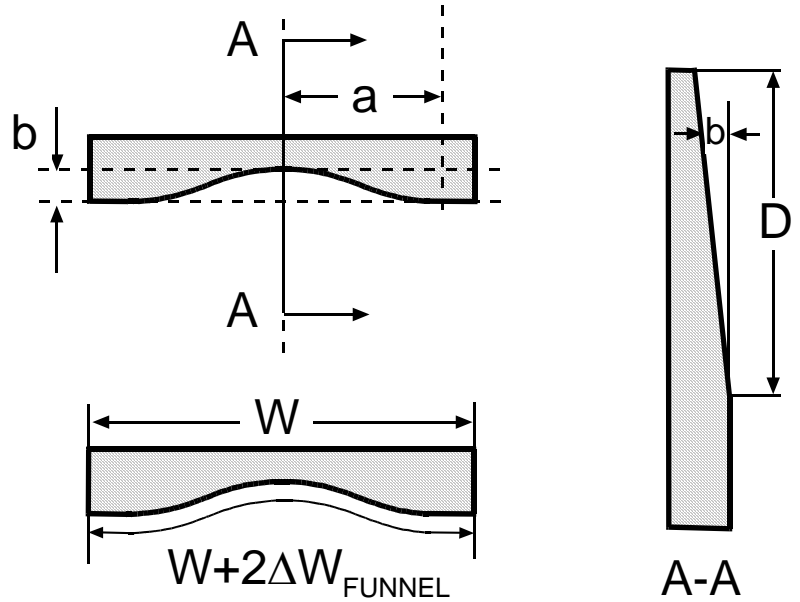
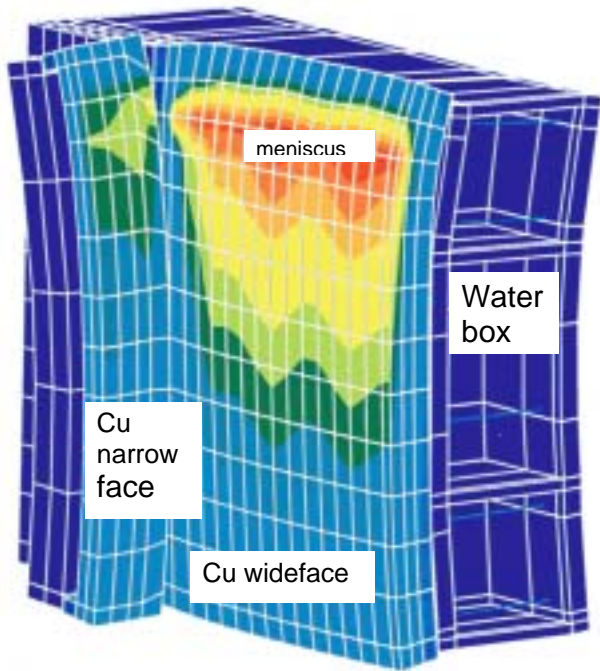


Fig. 6: Distortion in 1/4 standard slab mold, Fig. 7: Funnel mold shape description. (with computed temperature contours) [21]

Wide face distortion- The solidifying shell must navigate around the distorted wideface shape, whose maximum may exceed 1mm. This significant distortion greatly affects wideface taper, which helps to explain why widefaces are usually not tapered much. Simple calculations show, however, that this distortion has negligible effect on the shell width, so $\Delta W_{\text{WF-D}}$ can be ignored in narrowface taper design.

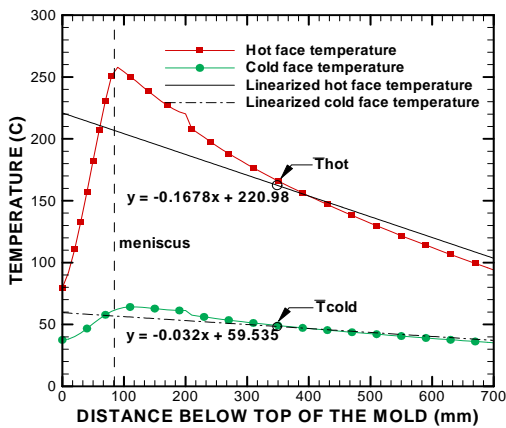


Fig. 8: Example temperatures for narrow face distortion calculation

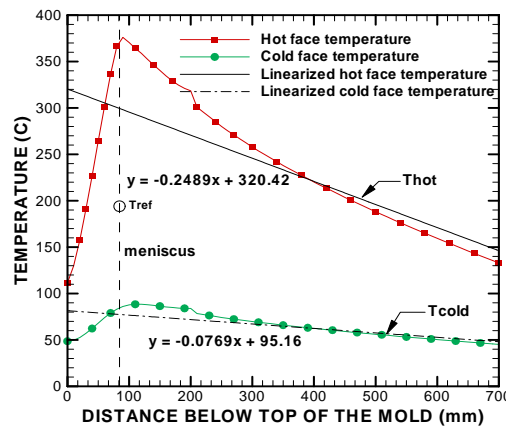


Fig. 9: Example temperatures for wideface expansion calculation

Effect of funnel-mold shape- In most thin slab casters there is a funnel-shaped cavity in the wide faces of the mold to allow the submerged entry nozzle to pour molten steel into the mold. This decrease in wideface perimeter with distance down the mold changes the ideal narrowface taper. It can be calculated from:

$$\Delta W_{FUNNEL} = \left\{ \left[\frac{a^2 + b^2}{2b} \sin^{-1} \left(\frac{2ab}{a^2 + b^2} \right) \right] - a \right\} \quad (8)$$

Where the funnel dimensions, shown in Fig. 7, in this work are a=1020 mm, b=60 mm, and D=750 mm

This contribution to mold taper is very important in most thin slab casters. For standard slab casting, with parallel plate mold walls, this term is naturally equal to zero.

Effect of flux-layer solidification- The solidified flux layer in the interfacial gap should increase in thickness with distance down the mold length, especially if it is continuous and attached to the mold wall. This is calculated by CON1D, as explained elsewhere^[15]. This effect represents an equivalent taper, and would allow less taper of the mold walls, if ΔW_{FLUX} is taken into account.

RESULTS

Simulations were performed to investigate the effects of casting speed, heat flux profile shape, powder composition, and steel grade on ideal taper. Further computations explore taper in funnel molds and during automated width changes. Taper is presented as %/mold unless otherwise specified. Sample results are given in Figs. 10-12 for a typical 200 mm thick slab mold, based on standard conditions of 1000 mm width, 800 mm working mold length, .07%C, 1.5m/min casting speed, and 1120 °C flux solidification temperature.

Figure 12 shows that thermal shrinkage strain is very large, dominating the need for taper. As for every case studied in this work, significantly more mold taper is needed just below the meniscus than near mold exit. Narrow face distortion tends to lessen ideal taper and to make the profile somewhat more linear, beyond 100mm below the meniscus. The increase in flux layer thickness down the mold appears to greatly lessen ideal taper. Flux layer stability is likely always difficult, however, so perhaps taper design should not rely on this effect. Wideface expansion has a similar trend, but not as large. Its effect can be lessened by careful adjustment of the screws to minimize backlash, or by the use of inclinometers during operation. Thus, ideal taper is presented both using Eq. 4, and using “shell shrinkage – mold distortion”, which neglects the flux layer and wideface expansion effects.

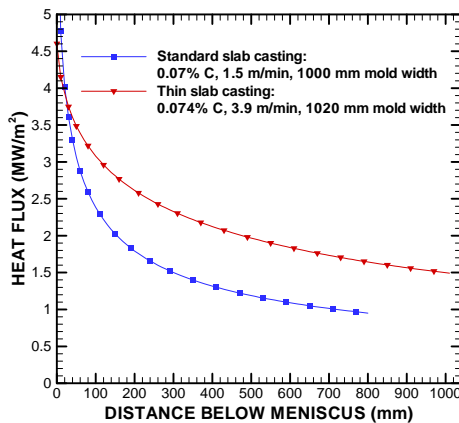


Fig. 10: Heat flux for standard (0.07%C at 1.5m/min) and thin slab casting (0.074%C at 3.9 m/min).

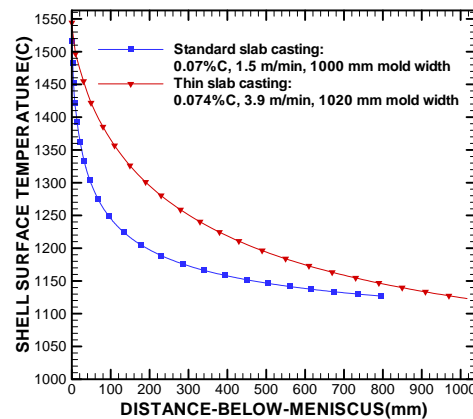


Fig. 11: Steel shell surface temperature for standard (0.07%C at 1.5m/min) and thin slab casting (0.074%C at 3.9 m/min).

Effect of funnel mold- Typical results for thin slab casting in a funnel mold are presented in Figs. 10, 11, and 13. Thin slab casting has higher casting speed (3.9 m/min) than conventional slab casting, so produces higher heat flux, higher surface temperature, and less shrinkage. The funnel has a huge effect in compensating the

need for taper, as shown in Fig. 13. The net result is that ideal taper is negative, meaning that the mold width at mold exit should be slightly wider than at the meniscus.

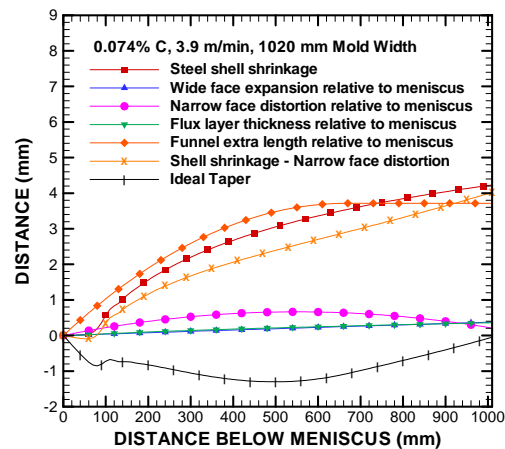
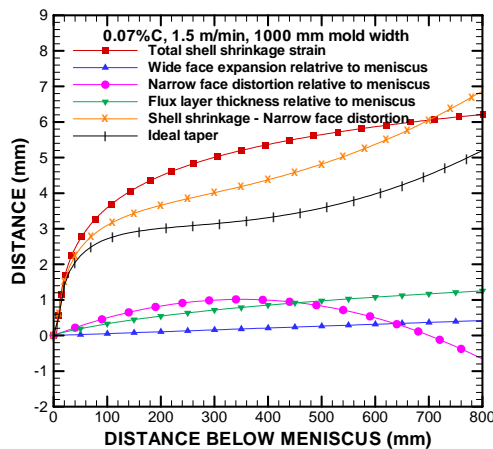


Fig. 12: Ideal taper for conventional slab casting conditions (0.07%C steel in Table I)

Fig. 13: Ideal taper for funnel-mold thin-slab casting (0.074%C and 3.9 m/min).

Effect of casting speed- The effect of casting speed is shown in Figs. 14 to19, for a typical low-carbon (0.07%C) steel. The conditions and results at mold exit are tabulated in Table I for different steel grades. Higher casting speed produces less dwell time in the mold, a higher surface temperature, less shell shrinkage, and less taper. The decrease in shrinkage is not as much as might be expected, however, because the higher average mold heat flux lowers the shell surface temperature (for a given time). The next effect of casting speed on shrinkage is thus relatively small, as seen in Fig. 17.

More important are the effects of mold distortion and flux layer changes. Increasing casting speed increases narrowface distortion, which tends to lessen ideal taper. Changes in flux layer thickness and wideface expansion, if present, would greatly lessen ideal taper, as seen by comparing Figs. 18 and 19.

Table I: Casting speed and steel grade study

Carbon content	0.07%			0.13%		0.27%		0.47%		
%Mn, %Si	.3%, .03%			.57%, .22%				.75%, .22%		
Mold flux viscosity at 1300C (Pa-s)	0.083			0.192		0.083		0.083		
Flux solidification Temperature (C)	1120			1215		1120		1120		
Casting Speed (m/min)	1.1	1.5	1.9	1.2	1.5	1.2	1.5	1.04	1.3	1.5
Tundish temp (C)	1567			1555		1559		1542		1567
Heat Flux (MW/m²), Q(Eq.3)	1.39	1.61	1.80	1.16	1.29	1.48	1.65	1.39	1.54	1.64
Surface Temp mold exit (C)	1127	1127	1132	1238	1241	1113	1117	1095	1093	1115
Shrinkage 50mm below meniscus CON2D	2.85	2.73	2.73	1.81	1.62	2.42	2.07	2.30	1.95	2.31
Shrinkage mold exit (mm) CON2D	6.28	6.21	6.14	4.09	3.93	5.45	5.20	4.99	4.84	4.35
Shrinkage mold exit (%/mold) CON2D	1.26	1.24	1.23	0.82	0.79	1.09	1.04	1.00	0.97	0.87
Flux layer relative to meniscus (mm)	1.47	1.25	1.14	2.34	2.07	1.53	1.36	1.44	1.35	1.51
NF distortion relative to meniscus(mm)	-0.57	-0.66	-0.74	-0.47	-0.53	-0.61	-0.66	-0.56	-0.64	-0.68
WF expansion relative to meniscus (mm)	0.40	0.42	0.45	0.29	0.33	0.42	0.41	0.37	0.44	0.43
Ideal Taper mold exit (mm)	4.98	5.20	5.29	1.93	2.07	4.11	4.09	3.75	3.68	3.09
Ideal Taper mold exit (%/mold)	1.00	1.04	1.06	0.39	0.41	0.82	0.82	0.75	0.74	0.62
Shell shrinkage - NF distortion (mm),exit	6.85	6.87	6.88	4.56	4.46	6.05	5.86	5.55	5.48	5.03
Shell shrinkage - NF distortion (%/mold)	1.37	1.37	1.38	0.91	0.89	1.21	1.17	1.11	1.10	1.01

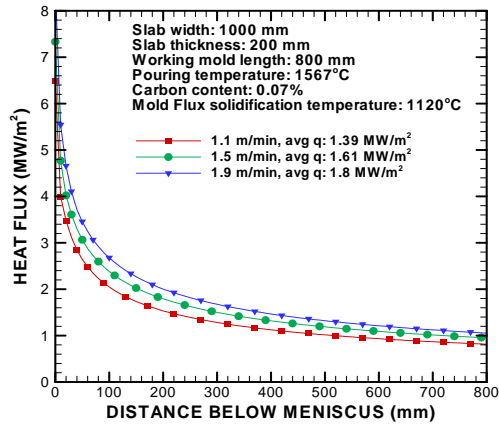


Fig. 14: Heat Flux profiles for different casting speeds, (0.07 %C conditions in Table I)

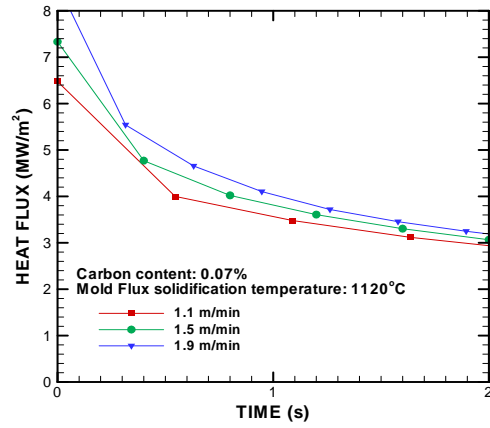


Fig. 15: Heat flux profile with time, detailing the first 2 seconds 0.07 %C conditions in Table I)

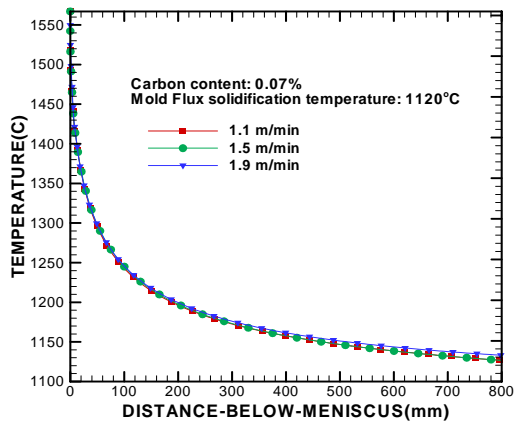


Fig. 16: Shell surface temperature for different casting speeds (0.07 %C conditions in Table I)

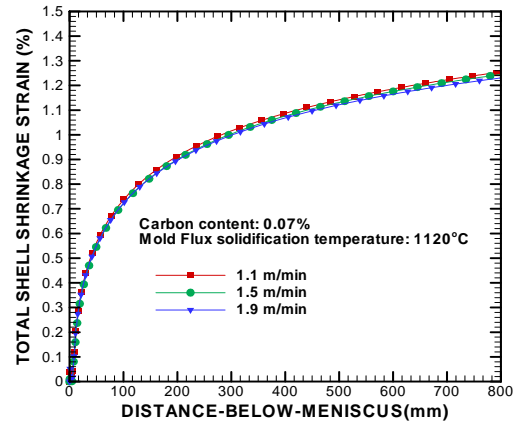


Fig. 17: Total shell shrinkage for different casting speeds (0.07 %C conditions in Table I)

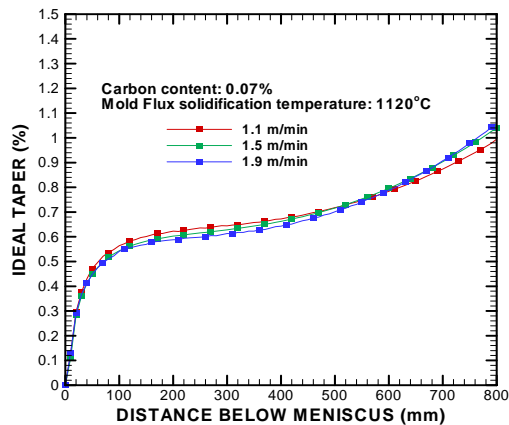


Fig. 18: Ideal taper for different casting speeds (0.07 %C conditions in Table I)

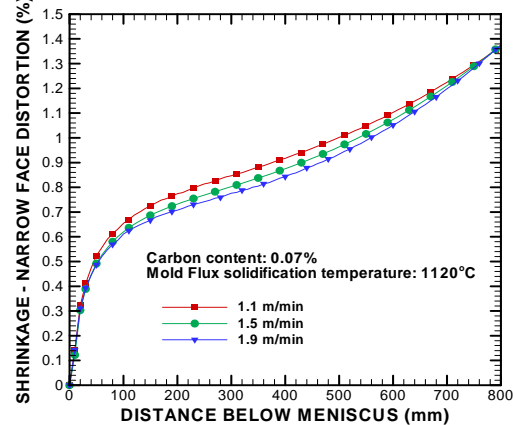


Fig. 19: shell shrinkage - narrowface distortion for different speeds (0.07 %C conditions in Table I)

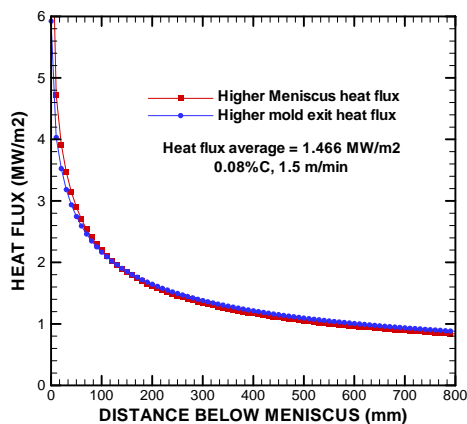


Fig. 20: Heat flux profiles with minor variations in curve shape

slightly higher heat flux near the top of the mold, while the other has slightly higher heat flux in the lower portions of the mold. Fig. 21 shows the corresponding temperature profiles, which are colder for the higher meniscus heat flux case. Fig. 22 shows that the corresponding shrinkage profiles differ much more. Specifically, the case with a higher initial heat flux, followed by a sharper drop produces more shrinkage at mold exit. This means that ideal taper depends on both the magnitude and shape of the heat flux curve. Because heat flux near the top of the mold is difficult to control, it would be wise to design the mold with some means to accommodate casting with non-optimal taper in that region

Effect of mold length- Longer molds naturally need more taper (per mold), owing to the extra cooling and shrinkage from the extra dwell time, but need less taper (per meter) owing to decreasing heat flux further below the meniscus. For a given set of conditions (same steel grade, same mold powder and same casting speed), the shrinkage profiles for different mold lengths all collapse onto a single curve. Results for any shorter mold length can be found simply by truncating the curve at the desired working mold length. This is possible because the heat flux function chosen in this work is a function only of time in the mold, and the shrinkage is governed by the heat flux profile.

Effect of Heat Flux Curve Shape- Shell shrinkage is quite sensitive to minor changes in the heat flux profile, especially near the meniscus. For example, Fig. 20 shows two similar heat flux curves with the same average, but with slightly different shapes. One has

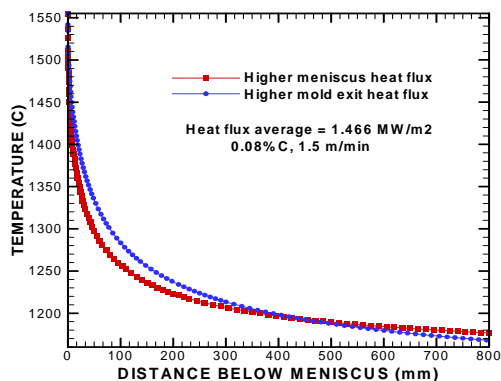


Fig. 21: Surface temperatures using heat flux curves in Fig. 20.

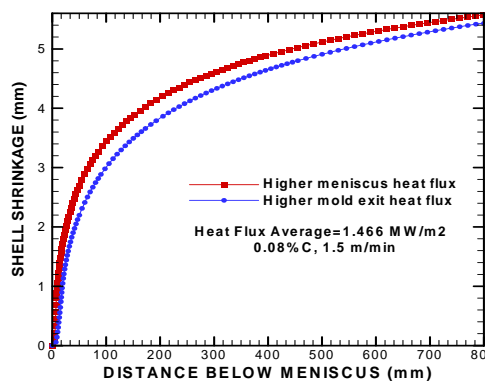


Fig. 22: Shrinkage predictions using heat flux curves in Fig. 20.

Effect of mold powder composition-The effect of mold powder composition is shown in Table II, Figs. 23 to 28. The change in mold powder composition is taken into account changing the powder viscosity and the solidification temperature. The most important is the effect of the solidification temperature. Increasing solidification temperature tends to lower the heat flux, (Fig. 23) owing to the thicker solid slag layer that forms. As a result the steel shell temperatures are higher, (Fig. 25) leading to less shell shrinkage (Fig. 26) and consequently lower ideal taper (Figs. 27 and 28).

Effect of Steel Grade-Ten simulations were conducted to study the effect of steel grades containing 0.07, 0.13, 0.27, 0.47% C, assuming mold powder properties typically used for each grade. Changing steel grade affects taper in two main ways, which tend to offset each other somewhat. Firstly, it changes the steel thermal and mechanical properties, most notably the thermal expansion, which is larger for peritectic steels, as seen in Fig. 4. Secondly, it affects the mold heat flux, which is 20% lower for peritectic steels (Eq. 3, Table I, and Fig. 29), due to deeper oscillation marks, and the higher solidification temperature of the mold flux used for these grades.

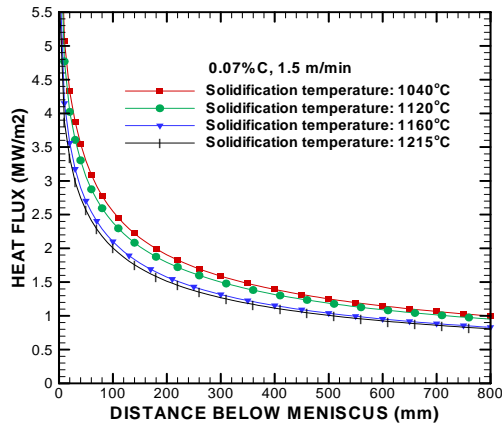


Fig. 23: Heat flux profiles for different mold flux solidification temperatures (Table II conditions)

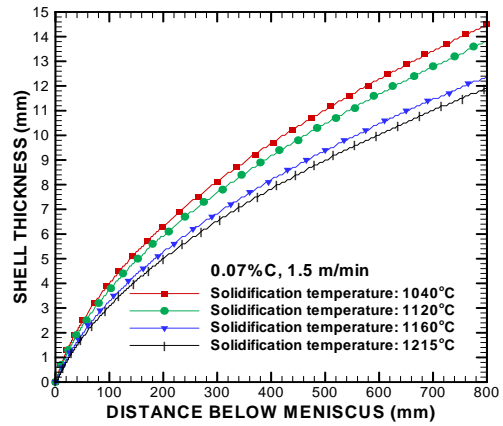


Fig. 24: Effect of powder composition on shell thickness (Table II conditions)

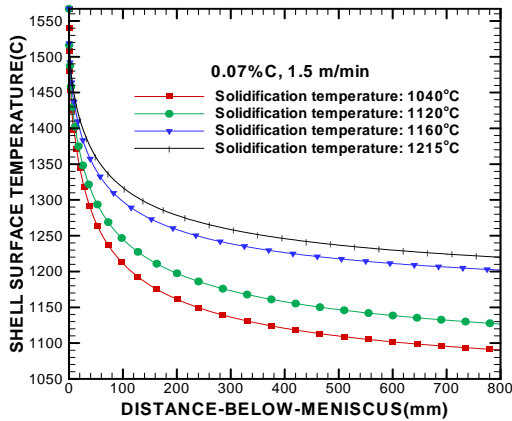


Fig. 25: Effect of powder composition on shell surface temperature (Table II conditions)

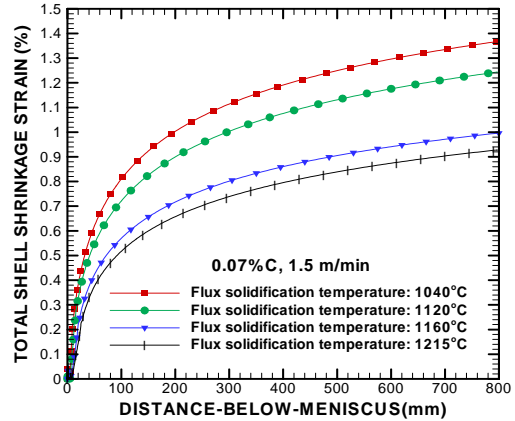


Fig. 26: Effect of powder composition on total shell shrinkage strain (Table II conditions)

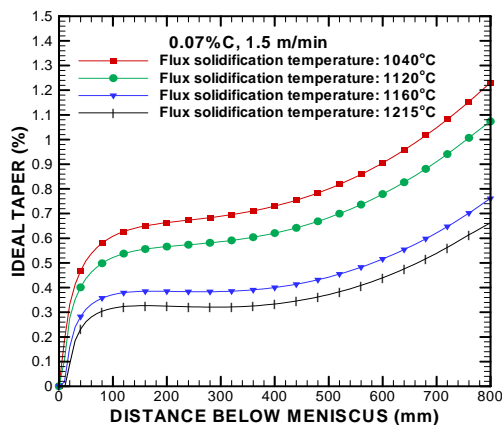


Fig. 27: Effect of powder composition on Ideal Taper (Table II conditions)

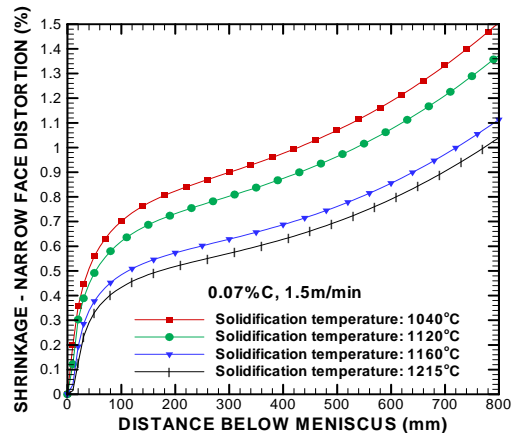


Fig. 28: Effect of powder composition on shrinkage - narrow face distortion (Table II conditions)

Table II: Mold powder composition study

Steel grade	low carbon (0.07%C, 0.3%Mn, 0.03%Si)			
Mold flux Viscosity at 1300C (Pa-s)	0.115	0.083	0.225	0.192
Flux solidification Temperature (C)	1040	1120	1160	1215
Casting Speed (m/min)	1.5	1.5	1.5	1.5
Tundish temp (C)	1567	1567	1567	1567
Heat Flux (MW/m²), Q(Eq.3)	1.71	1.61	1.41	1.36
Surface Temp mold exit (C)	1090	1127	1202	1220
Shrinkage 50mm below meniscus CON2D	3.08	2.73	2.12	1.88
Shrinkage mold exit (mm) CON2D	6.82	6.21	4.98	4.64
Shrinkage exit (%/mold) CON2D	1.36	1.24	1.00	0.93
Flux layer relative to meniscus (mm)	1.12	1.25	1.59	1.73
NF distortion relative to meniscus(mm)	-0.70	-0.66	-0.58	-0.56
WF expansion relative to meniscus (mm)	0.43	0.42	0.33	0.35
Ideal Taper mold exit (mm)	5.97	5.20	3.64	3.12
Ideal Taper mold exit (%/mold)	1.19	1.04	0.73	0.62
Shell shrinkage - NF distortion (mm), exit	7.52	6.87	5.56	5.20
Shell shrinkage - NF distortion (%/mold), exit	1.50	1.37	1.11	1.04

The practice of adopting mold powders with high solidification temperature and low viscosity was proposed by Wolf to produce lower, but more uniform heat transfer rates to help avoid cracks in depression-sensitive grades, such as peritectic steels^[3]. Slags with opposite properties are used for low and high carbon steels, to help avoid sticker problems. Thus, this study used the 1215°C solidification temperature slag for the 0.13%C steel and 1120°C slag for the low and high carbon steels, which is typical of industrial practice.

The effects of steel grade, and its associated heat flux, on shell temperature, shell thickness, shrinkage and ideal taper are shown in Figs. 29 to 33. These figures show that the lower heat flux produces a hotter shell surface temperature. This effect appears to outweigh the importance of the extra shrinkage of the peritectic steels. Thus, peritectic steels experience less shrinkage and require less taper than either low or high carbon steels.

The low carbon steels (<.08%C) have extra plastic strain, owing to their microstructure being in the soft, rapidly creeping delta phase. This extra creep generated in the solid tends to lower the amount of shrinkage experienced by these grades. The net effect is that low carbon steels experience both heat flux and shell shrinkage that is greater than for the other grades.

Comparing the results in Table I at mold exit and 50 mm below meniscus indicates that most of the shrinkage occurs very near to the meniscus, especially for the peritectic grade. This is likely the reason for the great sensitivity of the shrinkage to the heat flux documented in the previous section.

TAPER DURING AUTOMATED WIDTH CHANGE

During an automated width change, taper should be changed dynamically so that the lateral movement of the narrow face walls matches the time for vertical movement of the shell down the mold. The procedure for a widening width change is illustrated in Fig. 34.

- 1) Taper should first be increased, (to tapered) by moving the top of the narrowface mold walls outward.
- 2) This constant high taper should be maintained while the mold plates move outwards (at speed V_w), until the desired wider mold width is reached.
- 3) Finally, the mold bottoms should be moved outward to decrease the taper back to the standard taper.

This procedure is reversed for a narrowing width change, as illustrated in Fig. 35.

- 1) Taper should first be decreased by moving the mold top inward.
- 2) Next, a constant low taper should be maintained while the mold plates are moving inwards.
- 3) Finally, the mold bottoms are moved inward to increase the taper back to the standard.

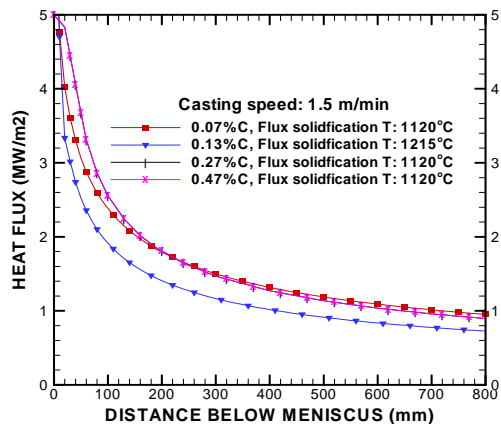


Fig. 29: Heat flux profiles for different steel grades (Table I conditions at 1.5m/min)

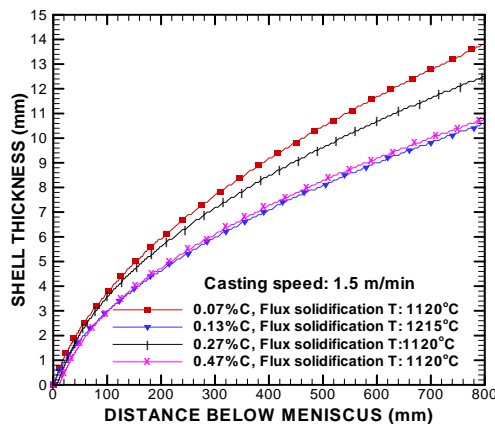


Fig. 30: Shell thickness for different steel grades (Table I conditions at 1.5m/min)

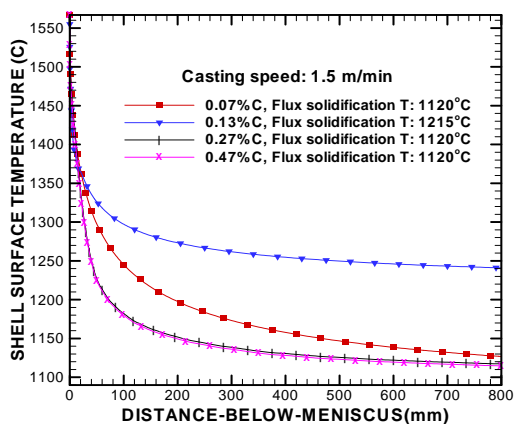


Fig. 31: Shell surface temperature for different steel grades (Table I conditions at 1.5m/min)

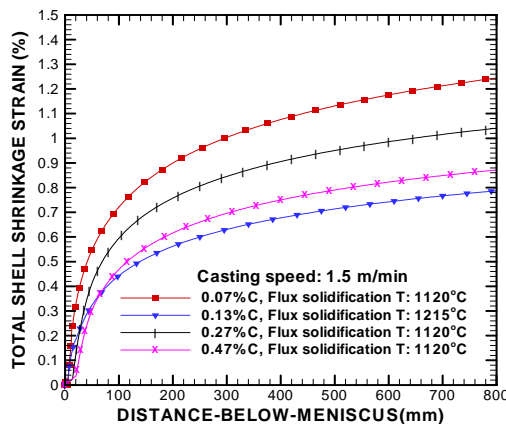


Fig. 32: Total shell shrinkage strain for different steel grades (Table I conditions at 1.5m/min)

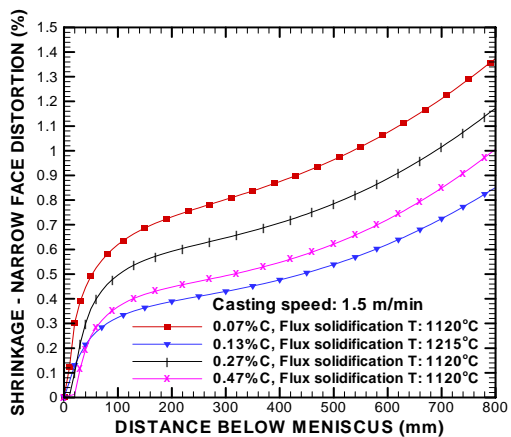


Fig. 33: Ideal taper for different steel grades (Table I conditions at 1.5m/min)

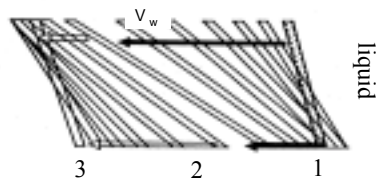


Fig. 34: Widening width change

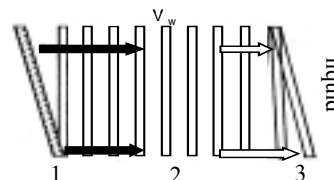


Fig. 35: Narrowing width change

The dynamic taper during the actual width change, $taper_d$ (%/m), should be chosen as follows [12]:

$$taper_d = taper_n - \frac{V_w}{V_c W} 100\%/m \quad (9)$$

Where $taper_n$ is the nominal taper during steady casting per unit length down mold (%/m) defined in Eq.(2), V_w is the lateral speed of narrow face movement during width change, V_c is the casting speed, W is the average mold width, ΔW is the difference in mold width between top and bottom of mold and L is the mold length. Note that an increasing width change causes negative V_w , meaning that the dynamic taper is larger than nominal.

CONCLUSIONS

Computational models have been applied to predict ideal narrowface taper during continuous casting of steel slabs. The models quantify ideal taper under a variety of conditions and reveal the following:

1. Ideal taper depends mainly on mold heat flux and is very sensitive to its profile, especially near the meniscus.
2. More taper is needed near the top of the mold, such as achieved using parabolic taper.
3. The funnel in thin slab molds greatly lowers the ideal narrowface taper.
3. Ideal taper decreases only very slightly with higher casting speed (for same conditions and heat flux profile).
4. Mold powders with higher solidification temperature have lower heat flux (compared with both oil lubrication or low solidification temperature powders) and consequently have less shrinkage and less ideal taper (other conditions staying the same).
5. Peritectic steels generally require less taper than either low or high carbon steels, owing to their lower heat flux.
6. Procedures are presented for changing taper dynamically during an automated width change, as a function of horizontal mold plate movement.

ACKNOWLEDGEMENTS

The authors thank the member companies of the Continuous Casting Consortium at the University of Illinois at Urbana-Champaign and Labein Technological Center in Bilbao, Spain. Authors also are grateful to Chunsheng Li for his work with the CON2D program and Ya Meng for work with the CON1D program.

REFERENCES

1. M.M. Wolf, "Mold Oscillation Guidelines," in Mold Operation for Quality and Productivity, A. Cramb, ed. ISS, Warrendale, PA, 1992, 15-35.
2. M. Wolf, "Mold Length in Slab Casting - a Review," Iron and Steelmaker, Vol. 23 (2), 1996, 41-51.
3. M.M. Wolf, Continuous Casting: Initial Solidification and Strand Surface Quality of Peritectic Steels, Vol. 9, Iron and Steel Society, Warrendale, PA, 1997, 1-111.
4. G.D. Lawson, S.C. Sander, W.H. Emling, A. Moitra, B.G. Thomas, "Prevention of Shell Thinning Breakouts Associated with Widening Width Changes," in Steelmaking Conf. Proc., Vol. 77, ISS, Warrendale, PA, (Chicago, IL), 1994, 329-336.
5. B.G. Thomas, A. Moitra and R. McDavid, "Simulation of Longitudinal Off-Corner Depressions in Continuously-Cast Steel Slabs," ISS Transactions, Vol. 23 (4), 1996, 57-70.
6. B.G. Thomas, A. Moitra and W.R. Storkman, "Optimizing Taper in Continuous Slab Casting Molds Using Mathematical Models," in Proceedings, 6th International Iron and Steel Congress, Vol. 3, Iron & Steel Inst. Japan, Tokyo, (Nagoya, Japan), 1990, 348-355.
7. R. Dippenaar, I.V. Samarasekera and J.K. Brimacombe, "Mold Taper in Continuous Casting Billet Machines," Iron and Steelmaker (ISS Transactions), Vol. 7, 1986, 331-343.
8. M. Larrecq and e. al, Report No. 941, IRSID, 1982.
9. B.G. Thomas and W.R. Storkman, "Mathematical Models of Continuous Slab Casting to Optimize Mold Taper," in Modeling and Control of Casting and Welding Processes - IV, A.F. Giamei and G.J. Abbaschian, eds., TMS, Warrendale, PA, (Palm Coast, FL), 1988, 287 - 297.

10. M.R. Ridolfi, B.G. Thomas, G. Li, U.D. Foglia, "The optimization of mold taper for the Ilva-Dalmine round bloom caster," in Continuous Casting, Vol. 9, ISS, Warrendale, PA, 1997, 259-269.
11. C. Li and B.G. Thomas, "Ideal Taper prediction for Billet Casting," in Steelmaking Conf. Proc., Vol. 86, ISS, Warrendale, PA, (Indianapolis, IN), 2003.
12. A. Moitra and B.G. Thomas, "Application of a Thermo-Mechanical Finite Element Model of Steel Shell Behavior in the Continuous Slab Casting Mold," in Steelmaking Proceedings, Vol. 76, Iron and Steel Society, (Dallas, TX), 1993, 657-667.
13. B.G. Thomas and H. Zhu, "Thermal Distortion of Solidifying Shell in Continuous Casting of Steel," in Proceedings of Internat. Symposia on Advanced Materials & Tech. for 21st Century, I. Ohnaka and D. Stefanescu, eds., TMS, Warrendale, PA, (Honolulu, HI), 1996, 197-208.
14. C. Li and B.G. Thomas, "Maximum Casting Speed for Continuous Cast Steel Billets Based on Sub-Mold Bulging Computation," in Steelmaking Conf. Proc., Vol. 85, ISS, Warrendale, PA, (Nashville, TN), 2002, 109-130.
15. Y. Meng and B.G. Thomas, "Heat Transfer and Solidification Model of Continuous Slab Casting: CON1D," Metal. & Material Trans., 2003,
16. C. Cicutti, MartinValdez, T. Perez, G. DiGresia, W. Balante, J. Petroni. Mould Thermal Evaluation in a Slab Continuous Casting Machine. Steelmaking Conference Proceedings. Vol. 85 (2002), 97-107.
17. P. Kozlowski, B.G. Thomas, J. Azzi, H. Wang, "Simple Constitutive Equations for Steel at High Temperature," Metall. Trans. A, Vol. 23A (3), 1992, 903-918.
18. P.J. Wray, "Plastic Deformation of Delta-Ferritic Iron at Intermediate Strain Rates," Metall. Trans. A, Vol. 7A (Nov.), 1976, 1621-1627.
19. T. Suzuki, K.H. Tacke, K. Wunnenberg, K. Schwerdtfeger, "Creep Properties of Steel at Continuous Casting Temperatures," Ironmaking Steelmaking, Vol. 15 (2), 1988, 90-100.
20. B.G. Thomas, A. Moitra and R. McDavid, "Simulation of Longitudinal Off-Corner Depressions in Continuously-Cast Steel Slabs," in Continuous Casting, Vol. 9, ISS, Warrendale, PA, 1997, 337-350.
21. B.G. Thomas, G. Li, A. Moitra, D. Habing, "Analysis of Thermal and Mechanical Behavior of Copper Molds during Continuous Casting of Steel Slabs," Iron and Steelmaker (ISS Transactions), Vol. 25 (10), 1998, 125-143.
22. E.C. Lemmon, "Multidimensional Integral Phase Change Approximations for Finite Element Conduction Codes," in Numerical Methods in Heat Transfer, R. Lewis, ed. John Wiley and Sons Ltd., (New York, NY), 1981, 201-213.

APPENDIX: STEEL THERMAL PROPERTIES

Thermal conductivity and enthalpy assumed as a function of temperature and steel grade are given in Figs. A-I and II. The nonlinear enthalpy gradients that accompany latent heat evolution were handled using a spatial averaging method by Lemon^[22].

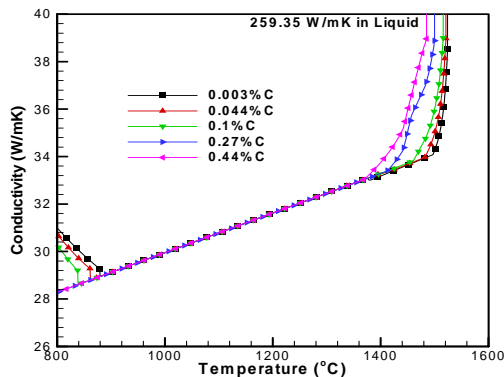


Fig. A- I: Thermal Conductivity of Steel

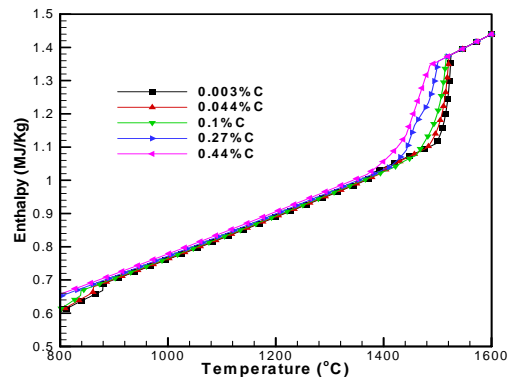


Fig. A- II: Enthalpy for Plain Carbon Steels